Karst cavity detection in carbonate rocks by integration of high resolution geophysical methods

Bakhtiar Qader Aziz[*], Peshawa Mohammad Ali[**]

[*] University of Sulaimani, Faculty of Science and Education Science, Dept. of Geology, bakhtiar_61@yahoo.com.

[**] University of Sulaimani, Faculty of Humanitarian Science, Dept. of Geography

Abstract:

Combined surveys using Ground Penetrating Radar (GPR) and Electrical Resistivity Tomography (ERT) are deployed to provide a cost effective characterization of the subsurface karst environments. A total of 12 GPR traverses and 4 ERT lines with lengths from 140 to 710 m are conducted at Sulaimani governorate, NE Iraq (45º 04' E and 35º 35' N). The area represents a broad syncline of limestone rocks, which is covered by a thin layer of recent sediments. Great anomaly depicting crest (high) like pattern was noticed on GPR records. A plausible interpretation for this anomaly was a cavity filled either by groundwater or by residual products of karstification. The presence of this cavity was confirmed also by electrical resistivity tomography. An excellent correlation exists between GPR signatures and ERT layers. The extension and the depth to the top of the cavity were determined from both GPR data and 2D inversion interpretation. A huge cave was discovered. It is located at depth of 25.0 meters. It has an elongated shape that extends from southeast to northwest direction. The geophysical survey results show this cave with approximate dimensions of 150.0 m long, 35.0 m wide and 24.0 m high.

Keywords: Carbonate Cave; GPR; Resistivity Tomography

I. Introduction

Several locations in Sulaimani governorate/Iraqi Kurdistan Region have less than 25.0 m of overburden soil over a thick carbonate (limestone) platform, with rock outcrops in many areas. It is often weathered near its surface. It contains fissures and solution channels that provide conduits for the vertical flow of surface water into the underlying aquifer(s). Organic and carbonic acids in the surface runoff further dissolve the limestone and enlarge the conduits. Sulaimani's annual precipitation normally exceeds 500 mm per year and, combined with seasonal fluctuations in groundwater levels; it often accelerates the process of dissolving process.

A variety of geophysical techniques can be used to detect the presence of the subsurface caves and voids. All of them are based on a physical contrast between a cave and the surrounding rocks. The difference in resistance between water (or clay)-filled cavity and the surrounding limestone may be the most outstanding physical feature of a cave. So the study aims to find out the possibility of integrating the GPR and ERT methods for identification of underground cavities. More emphasis is being placed on integrated surveys, in which two or more complementary methods are combined to constrain an interpretation.

The GPR technique is similar in principle to seismic reflection and sonar techniques. Pulse-mode GPR systems radiate short pulses of high frequency (10-2000 MHz) electromagnetic energy into the ground from a transmitting antenna. The propagation of the radar signal depends on the frequency-dependent electrical properties of the ground. By exploiting the wave propagation characteristics of electromagnetic fields, GPR provides a very high resolution sub-surface mapping method. It is a very useful geophysical method for use in hydrogeology and near surface mapping studies (Kim et al., 2000) as well as it is useful method for shallow engineering investigations (Morey, 1974; Ulriksen, 1982; Ballard, 1983). One of the main applications for GPR technique is cavity and fracture detection (Leggo and Leech, 1983, Leggo,1982; McCann et. al., 1988; Sasahara et. al., 1995; Valle and Zanzi, 1996; El-Behiry and Hanafy, 2000; Hruska and Hubatka, 2000; Pipan et al., 2000).

II. Geology and Structural Setting:

The study area is about 20 km west of Sulaimani City, NE IRAQ (Figure 1) and basically consists of Quaternary alluvium overlying the Pilaspi limestone formation. The alluvial deposits generally consist of very soft to firm clay and silty clay up to a depth of 1-15 m with some lenses of gravel. The Pilaspi Formation was deposited in the late Lower Eocene-Upper Eocene cycle and in shallow lagoon environment. It is composed of two parts; the upper part is well-bedded, bituminous, chalky and crystalline limestone with bands of white chalky marl and chert nodules toward the top. The lower part shows well-bedded hard porous or vitreous bituminous, poorly fossiliferous limestone with algal or shell section. The thickness varies roughly between 100.0 to 200.0 meters (Buday, 1980).

Structurally, the area is an elongated syncline that extends NW -SE direction and for about 30.0 kms. The syncline with is about 3.0 kms. (Figure 1). The area under consideration is affected by two sets of faulting systems striking mainly in NW-SE and NE-SW directions. Most of them are normal faults others are reversed. In addition to faults, at least three sets of joints dissect the area. These joints trend in NW-SE, E-W and NE-SW directions. Excavation, construction and quarrying processes, which are located very near to the investigated site, show many karstic features, such as cavities and sinkholes. These features are mainly associated with fracture zones, faults and joints are accelerating their formation (Aziz, 2005).

III. METHODOLOGY

Ground penetrating radar

The survey was carried out using a RAMAC2, GPR SYSTEM consisting of a Model PR- 8304 profiling recorder with automatic gain ranging, graphic, magnetic tape data recording and a copper-foil dipole antenna having a center operating frequency of 25 MHz. Data collection was carried by using 'Ground vision' software. The measurements were made along 11 lines in northwest- southeast direction (Figure 2). The length of the survey lines were ranging from 160 to 175 m. Data collected were processed using software (RadExp) to produce 2D radargram in time scale. Frequency filters and triple time varying gains were used to get good quality data Prior to producing the time section. All data was filtered for background removal and to remove the DC current effect and multiplied by gain functions to overcome the attenuation effect of the earth materials as well as to minimize the noise effects. Through using

RadExp software the data were filtered or "dewowed" to remove low frequency noise induced by the recording system. An automatic time zero adjustment was applied to each data set to compensate for instrument drift during recording, and also to correct small static (time) shifts in the direct wave first arrival. Next a trace equalizing AGC function was applied to scale the data, and to enhance deeper reflection signals. AGC scaling enhanced reflector continuity by increasing the amplitude of weak signals across small fractures and in karst areas. Since AGC scaling alters the amplitude information of the data and thereby obstructs stratigraphic interpretation, spherical and exponential compensation (SEC) was applied separately to examine the effects on amplitudes associated with certain stratigraphic anomalies. A velocity of 12 m/ns and an attenuation of 1 dB/m were used as estimates for limestone materials in order to compensate for spherical spreading and exponential attenuation of the electromagnetic energy.

Electrical Resistivity Tomography

In the ERT survey, measurements were made along 3 traverses trending in NW-SE directions as shown in Figure 2. The length of each survey line was 710 meters. Expected maximum depth of current penetration into the ground is approximately about 130 meters. SYSCAL Jr-72 Switch instrument from IRIS Company was used for the data collection. Wenner-Schlumberger array electrode configuration was used to provide a good horizontal and vertical resolution for a clear image of the cave. The data collected in the field was interpreted using the computer software RES2DINV, Ver. 3.3, (Loke and Barker, 1996) which automatically subdivide the subsurface into a number of blocks and then it uses a least-squares inversion scheme to determine the appropriate resistivity values for each block in 2-D. Geoelectrical imaging surveys are normally carried out with multi-electrode resistivity system. In this survey, a total of 72 electrodes are deployed in a straight line with constant spacing equal to 10 m and connected to a multi-core cable. A computer-controlled system (Griffith et al. 1990) is then used to select the active electrodes for each measurement. The data gathered in this survey was interpreted to provide an inverse resistivity section. Anomalies near the edge of models are also suspect since there are usually few data points available for the inversion in these areas. Different numbers of iterations with different inversion parameters are necessary to insure an anomaly near the edge is not a processing artifact. Some of the inversion parameters that may be changed to test a solution's robustness include damping factor, flatness, filters and the initial model for the inversion (Loke and Barker, 1996).

IV. INTERPRETATION, RESULTS AND DISCUSSION

In general, the radar sections show a very good penetration due to thin layer of soil cover which is less than one meter as well as high resistive limestone rocks of Pilaspi Formation beneath the soil cover. A number of anomalies, either as hyperbola patterns or discontinuous signals are more visible at the two way time of 100 to 300 nsec. At greater times, only one great anomaly appears, mainly in hyperbolic form, with strong reverberations, strictly under the apices. We believe that the hyperbolic anomalies are generated by reflection signals from a cave located in the limestone. For the purpose of the present study, we have

neglected the shallow anomalies, focusing our attention on the deeper ones.

Figures 6, 7 and 8 show an example of 2D radar gram section of Line 5, 7 and 8. Basically, the section can be divided into two particular reflection pattern representing different lithological units. At depth 0 to. 20 m, the reflections are flat continuous showing high amplitudes representing the Pilaspi layers, whereas at depth of 20 until 40 m it shows discontinuous and chaotic pattern the reflection is weak and unclear or sometimes called free-reflection zone which is representing a cave.

The final processed georadar profiles along with an interpretation are shown in Fig. 3 to Fig. 14. Interpretation of the georadar profiles identified one areas of karst which was present beneath the limestone bench. A clay-filled karst feature was interpreted to exist between lateral distances of zero to 175 m (See figures 7, 8 and 9). Several clay-filled cavities were exposed within the surrounding area due to excavation of the limestone rocks in the quarries of the Bazian cement factory.

The interpretation of the resistivity profiles was relatively straightforward in terms of differentiating and mapping lithologic units. Units with resistivities greater than 35 Ohm.m were mapped as limestone; units with resistivities less than 15 Ohm.m were mapped as moist soil or clay; units with resistivities greater than 15 Ohm.m but less than 35 Ohm.m were interpreted as transitional zones probably consisting of moderately to intensely fractured and/or weathered limestone with clay in-fill (Figures 15, 16 and 17).

ERT sections show resistivity variation from top to bottom with values ranging from 7 Ωm to almost 300 Ωm. The thickness of top soil consisting of clay to fine silt overlying the limestone layer varies from 1 to 40 m with resistivities ranging from 7 to 15 Ωm.

The inversion process converged with an RMS error varying between 3 and 7. There was not much difference in the inverted section for the last 3 iterations, so we choose the sections with the lowest RMS error. Generally, the inverted resistivity sections show that the site is characterized by relatively low resistivity soil cover ranging from 7 to 15 Ohm.m with an average value of about 15 Ohm.m. The resistivity sections of profiles 1,2 and 3 (Figs. 15,16 and 17) show one distinct anomaly of relatively low resistivity values at a lateral distance of approximately equal to 220 and 290 m from the starting point of measurements. The anomaly of 20.0 ohm.m is located at 18 meters depth and deeper (22.0 meters depth) at profile 2 and no extension at profile 3. Similar anomalous zones were detected in the profile 2 but with lateral extension to more than 175 m. According to the available geological and geoelectrical information, these anomalies are probably related to karst cavity in limestone rocks filled with weathered product of carstification. Moreover, linear abrupt changes in the resistivity distributions noticeable in the sections are mostly related to contacts between hard and fractured wet limestone as well as the other linear structures.

2D resistivity surveys clearly show the central depression as well as resistivity contrasts between the ambient rocks sediments within and outside of the cave. Clay-filled and water-filled cave is represented as high-conductivity (low resistivity) zone in the resistivity images. The low resistivities may be due to infilling by clay, or water within the cave.

Fig. 15,16 and 17 shows the example of inverted and resistivity models made from Wenner-Schlumberger surveys with 10m electrode spacing. In these figures the filled cave appears as a conductive (low resistivity) within resistive zone in the bedrock.

Depend on both 2D resistivity and GPR survey the exact boundary of the detected cave is plotted on the base map of the area as shown in Fig.18.

CONCLUSION

This paper investigates the applicability of Ground Penetrating Radar (GPR) and Electrical Resistivity Tomography (ERT) techniques for delineation of subsurface cavities in an area covered by limestone rocks. The study reveals to the following results:

1- A huge cave was discovered. It is located at depth of 25.0 meters. It has an elongated shape that extends from southeast to northwest direction. The geophysical survey results show this cave with approximate dimensions of 150.0 m long, 35.0 m wide and 24.0 m high.

2- GPR technique is most effectiveness in detecting the sharp boundary between the cave and the host rocks, while 2D resistivity technique the boundary represents by gradual decreasing of resistivity values.

3- 2D resistivity technique unable for identify a filling materials of the cave because both water and clay have the same influence on the resistivity values. Correspondingly detection of weak reflections from sediments by GPR technique (as observed in the radar sections) within the cave refers to the existence of clay sediments whenever if the cave filled by water zone of no reflections are appeared in the space of the cave.

4- Due to high resolution of the GPR technique several large stalactites were detected while detection of such features by 2D resistivity technique is impossible due to great smoothing of field data in the inversion process

References

Aziz, B.Q., 2005: Two dimention resistivity imagind tomography for hydrogeological study in Bazian basin-west sulaimani City,NE-IRAQ, Ph. D dissertation, Dept of Geology, Sulaimani University, Sulaimani.

Ballard, R.F., 1983: Cavity detection and delineation research Rep.5, Electromagnetic (radar) techniques applied to cavity detection, Tech. Rep. GL-83-1 U.S.Army Engr. Waterways Expr Station, Viksburg, MS.

Buday, T., 1980: the regional geology of Iraq. Vol-1, (Stratigraphy and Palegeography) GEOSURV, Baghdad, Iraq, 445P.

El-Behiry, M.G. and Hanafy, Sh. M., 2000: Geophysical surveys to map the vertical extension of sinkhole: a comparison study.: SAGEEP-2000,341 – 350.

Griffith, D.H., Turnbull, J. and Olayinka, A.I., 1990: Two-dimensional resistivity mapping with a computer controlled array. *First Break* 8: 121-129.

Hruska, J., Hubatka, F., 2000: Landslides investigation and monitoring by a high performance and cavities in limestone: GPR 2000 Proceedings of the 8th International Conference on Ground-Penetrating Radar, Gold Coast.

Kim C., Daniels, J.J., Guy, E.D., Radzevicius, S.J. & Holt, J. 2000: Residual hydrocarbons in a water-saturated medium: A detection strategy using ground penetrating radar. *Environmental Geosciences* 7(4): 169-174.

Leggo, P. J., 1982: Geological applications of ground impulse radar: Transactions of the Institute of Mining and Metallurgy; B: Applied Earth Science,91: B1-5.

Leggo, P. J. and Leech, C., 1983: Subsurface investigations for shallow mine workings and cavities by ground impulse radar technique:Ground Engineering, 16, 20-23.

Loke, M.H. & Barker, R.D. 1996: Rapid least-squares inversion of apparent resistivity pseudosection by a quasi –Newton method. *Geophysical prospecting* 44: 131-152.

McCann, D. M., Jackson, P. D. and Fenning, P. J., 1988: Comparison of the seismic and groundprobing radar methods in geological surveying:IEEE proceedings, 135 (F, 4), 380-390.

Morey, R.M., 1974: Continuous subsurface profiling by impulse radar, Proc. Engr. Foundation Conference Subsurface Exploration. Underground Excavation and Heavy construction, Am. Society Civil Engineers, 213-232.

Pipan, M., Baradello, L., Forte, E., and Prizzon, A.,2000: GPR study of bedding planes, fractures and cavities in limestone: GPR 2000 Proceedings of the 8th International Conference on Ground-Penetrating Radar, Gold Coast.

Sasahara, K., Tsuchida, T., and Fenner, T. J., 1995: An investigation of cracks in rock slope using ground penetrating radar: SAGEEP'95, 149-158.

Ulriksen, C.P., 1982: Application of impulse radar to civil engineering: Ph. D dissertation, Dept of EngineeringGeology, Lund University of Tech, Sweden.

Valle, S. and Zanzi, L., 1996: Radar tomography for cavities detection: SAGEEP'96, 555 - 563.

Fig (1) Location image of the area.

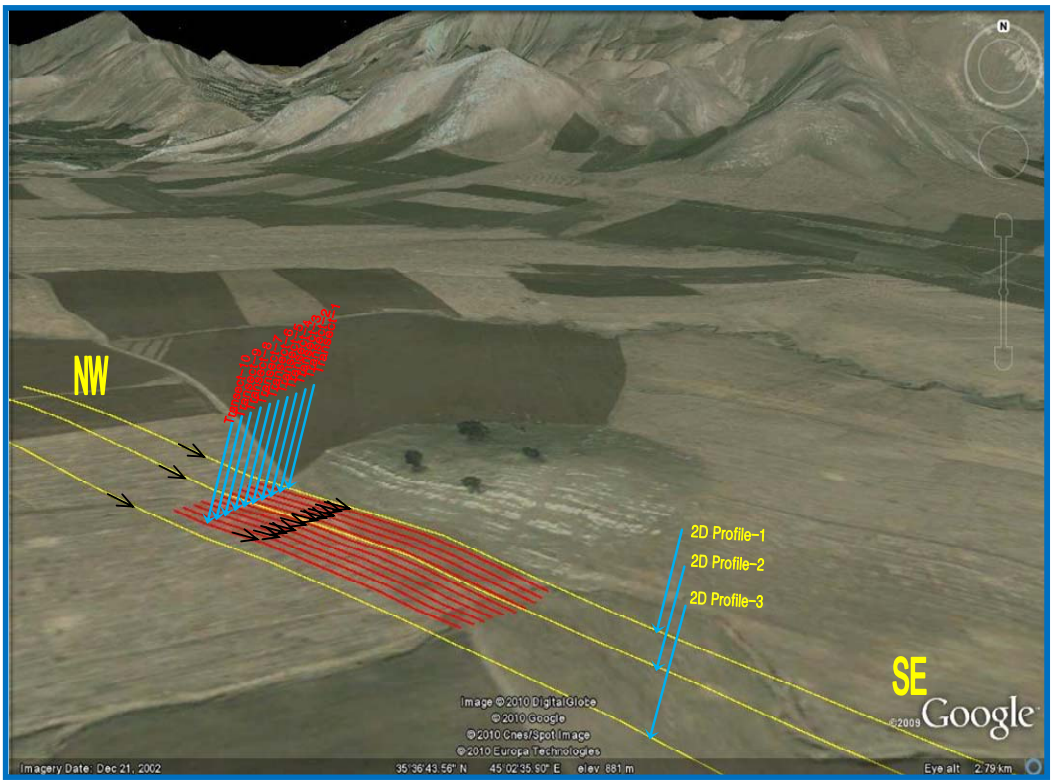

Fig (2) Location of the surveyed lines.

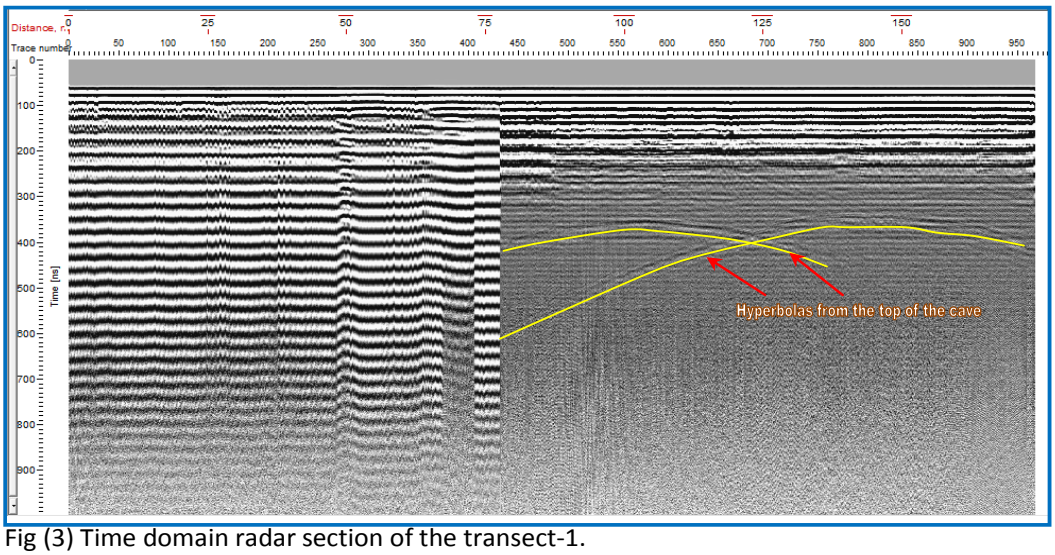

Fig (3) Time domain radar section of the transect-1.

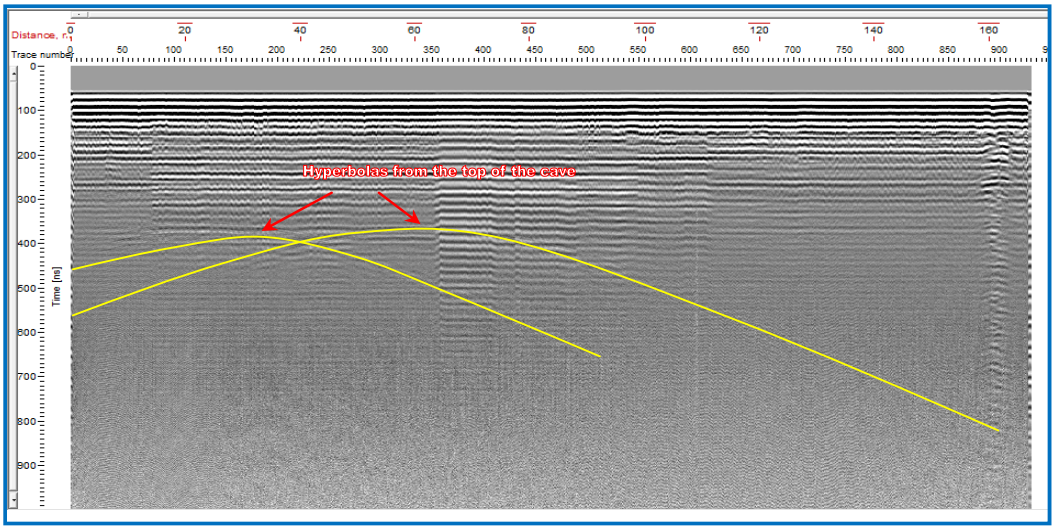

Fig (4) Time domain radar section of the transect-2.

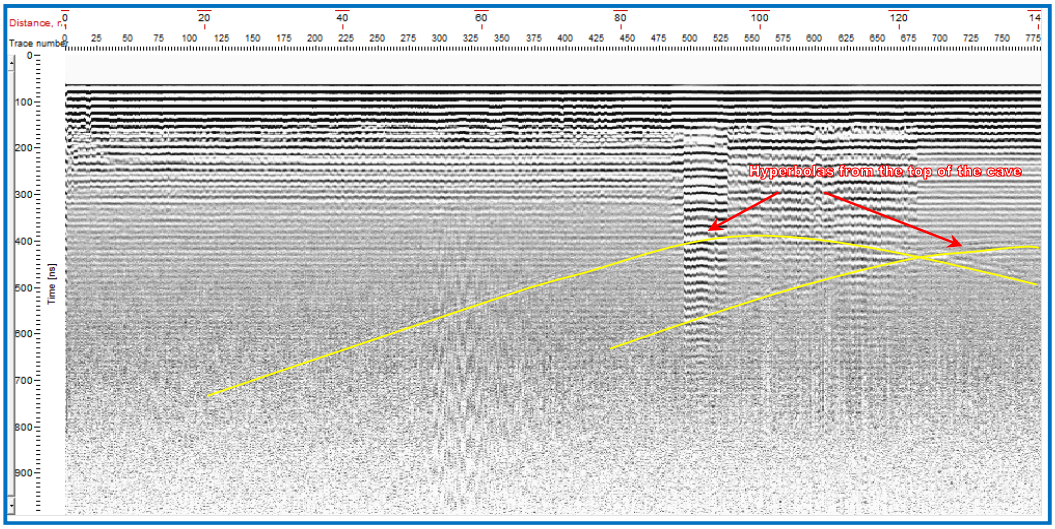

Fig (5) Time domain radar section of the transect-3.

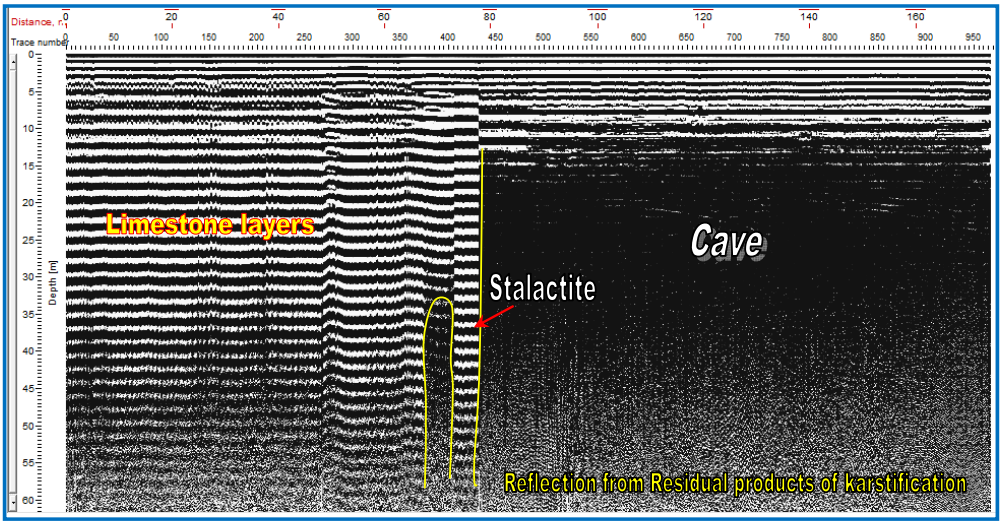

Fig (6) Depth section of the transect-1

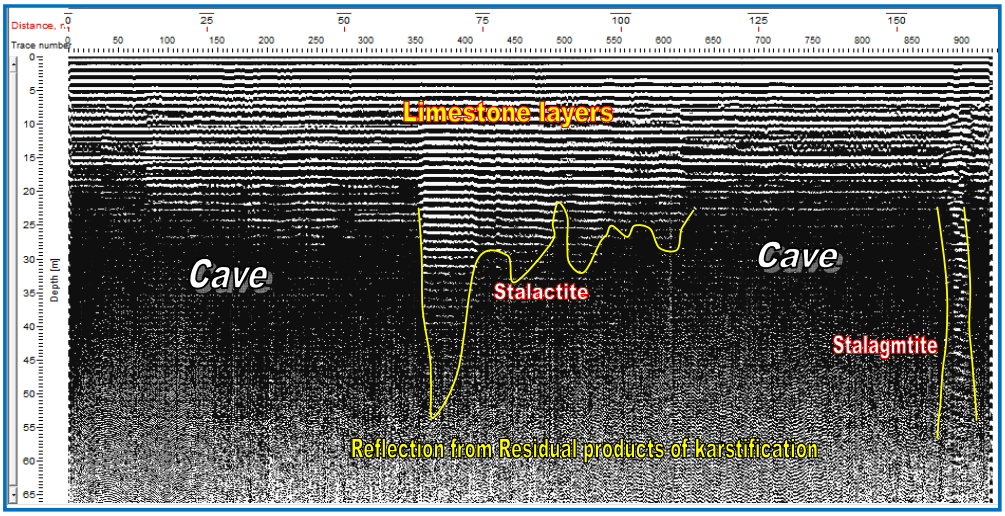

Fig (7) Depth section of the transect-2

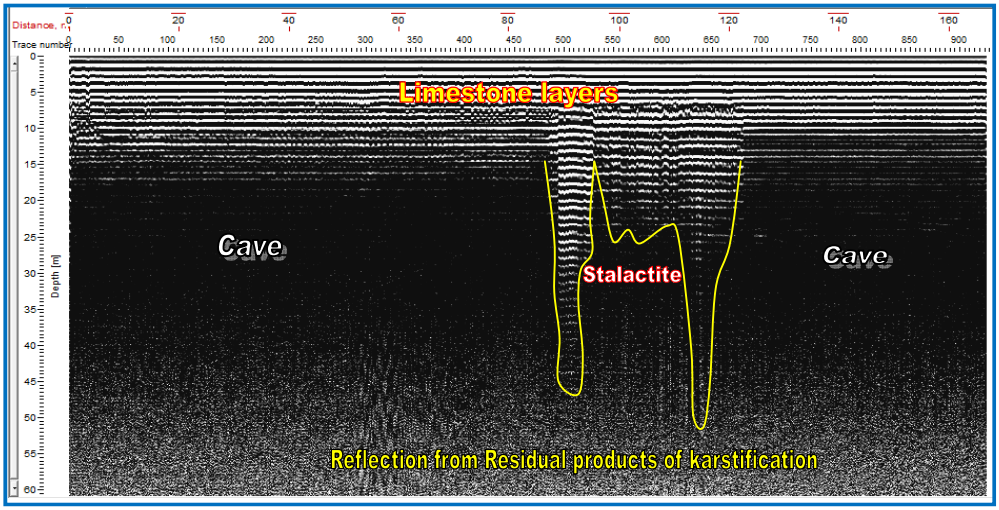

Fig (8) Depth section of the transect-3

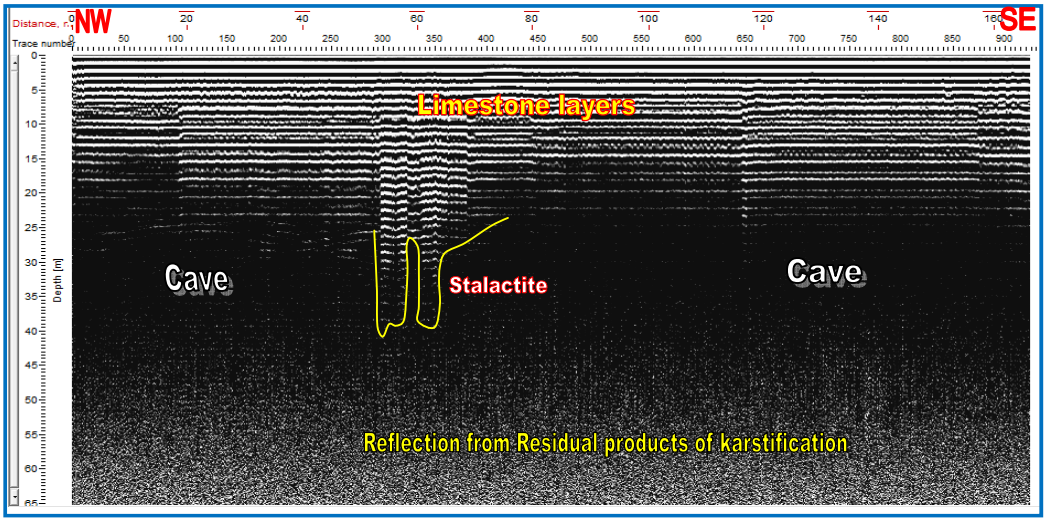

Fig (9) Depth section of the transect-4

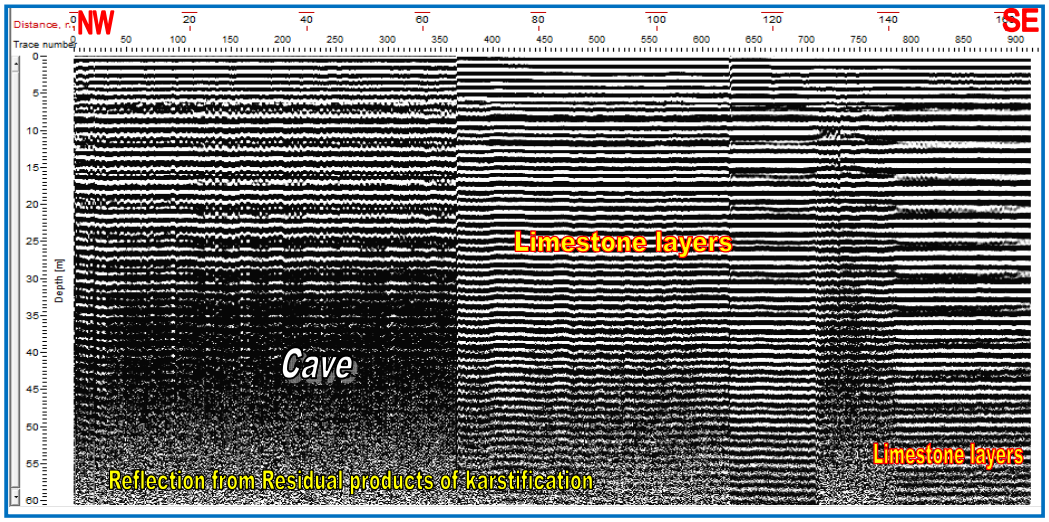

Fig (10) Depth section of the transect-5

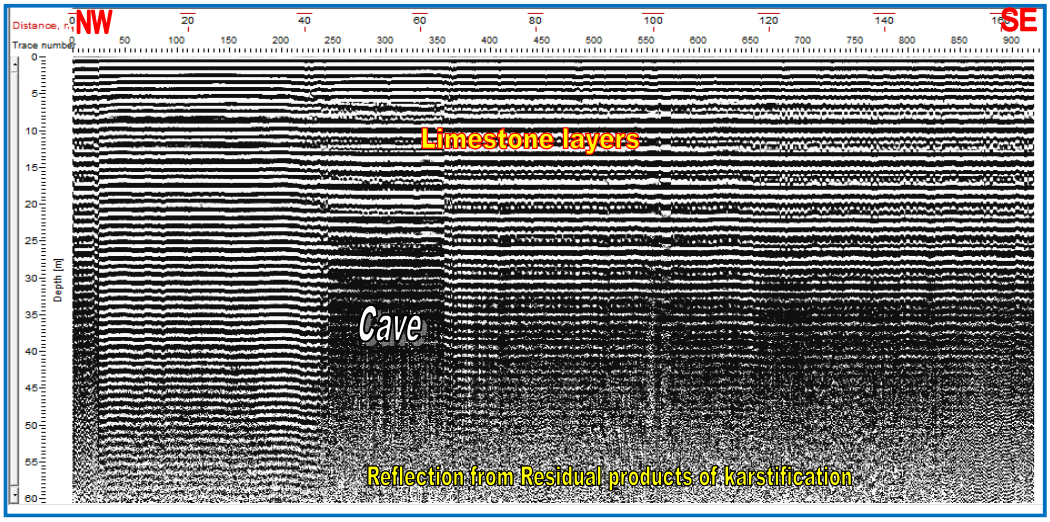

Fig (11) Depth section of the transect-6

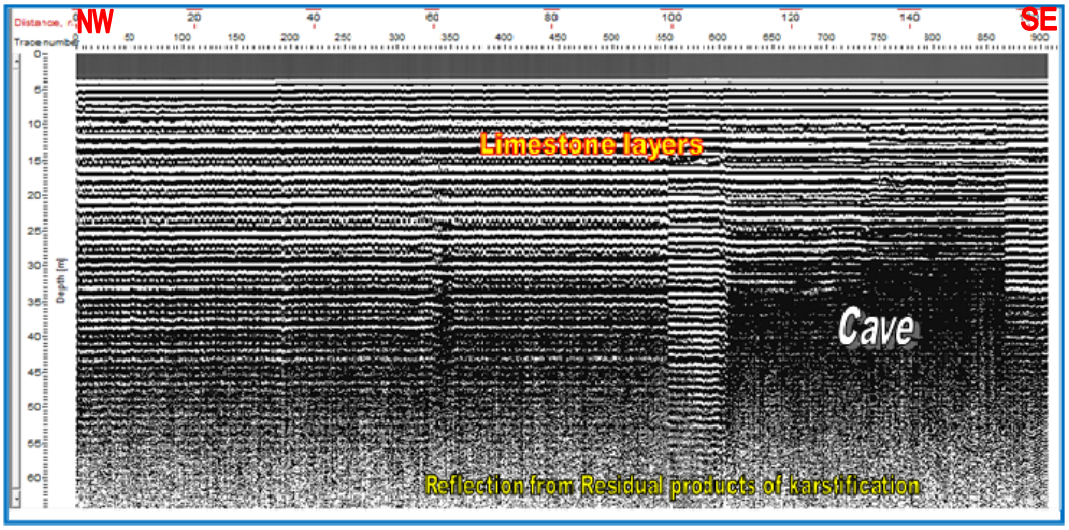

Fig (12) Depth section of the transect-7

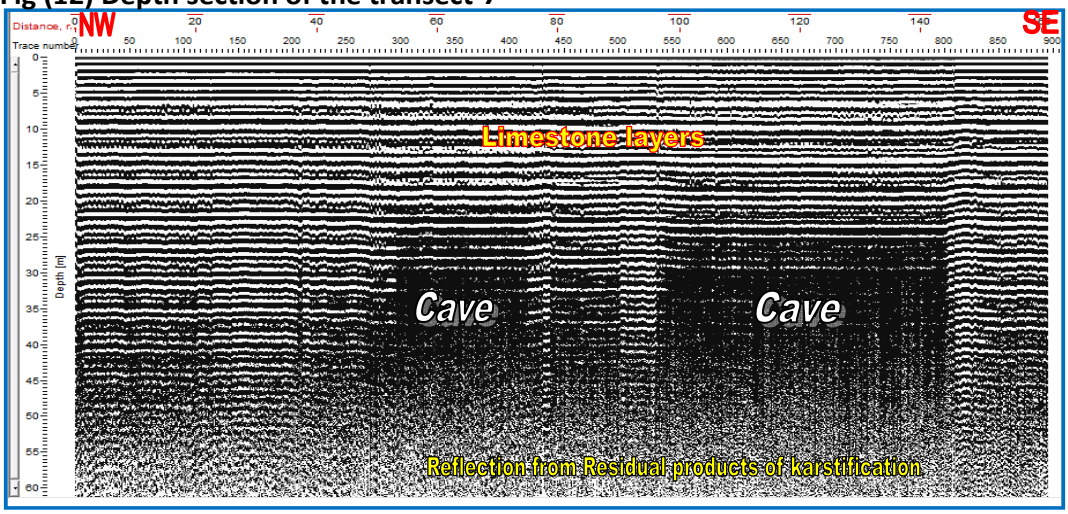

Fig (13) Depth section of the transect-9

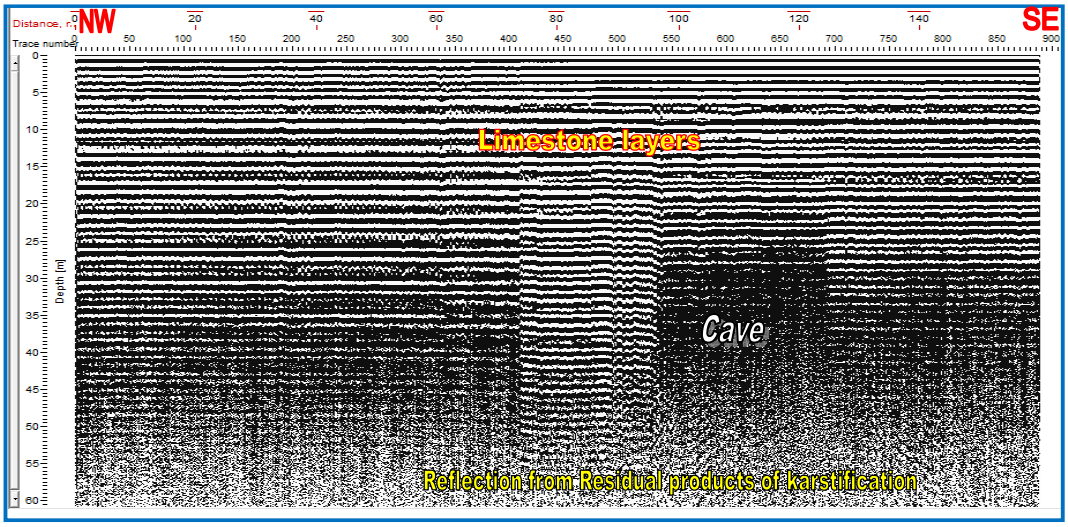

Fig (14) Depth section of the transect-10

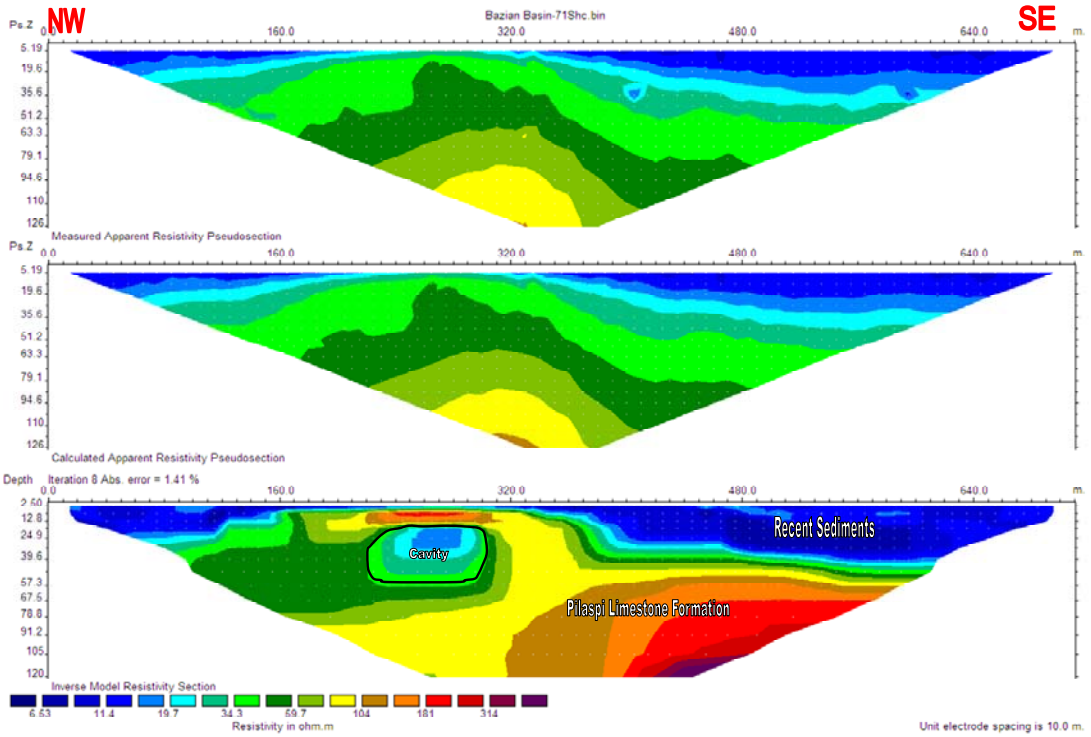

Fig (15) Inversion section of the profile-1

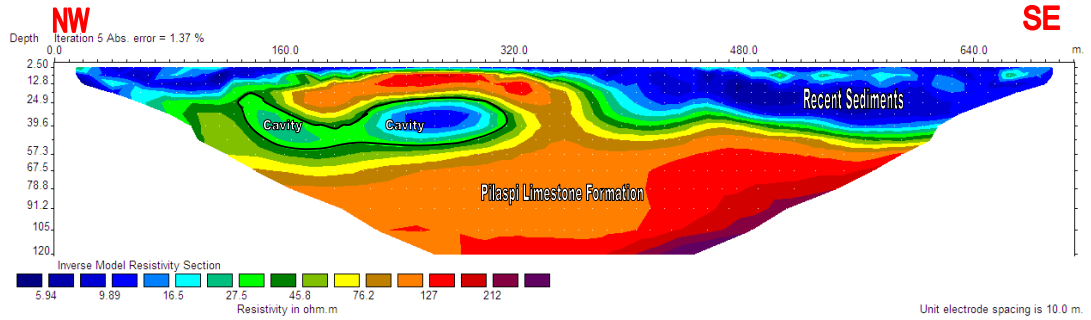

Fig (16) Inversion section of the profile-2

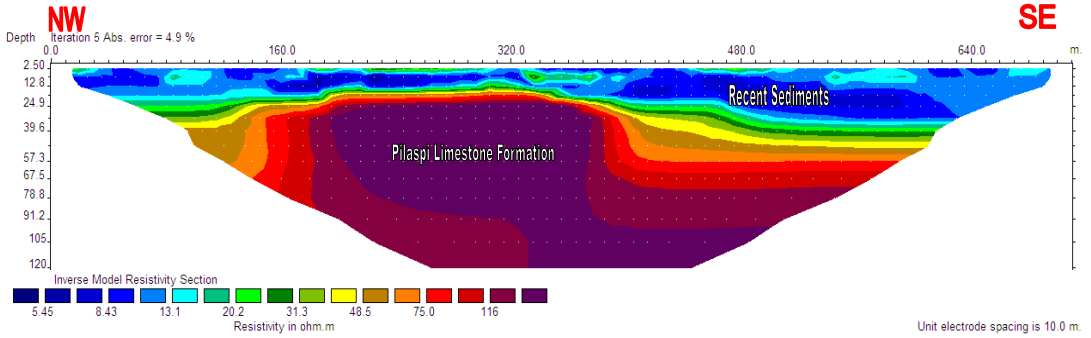

Fig (17) Inversion section of the profile-3

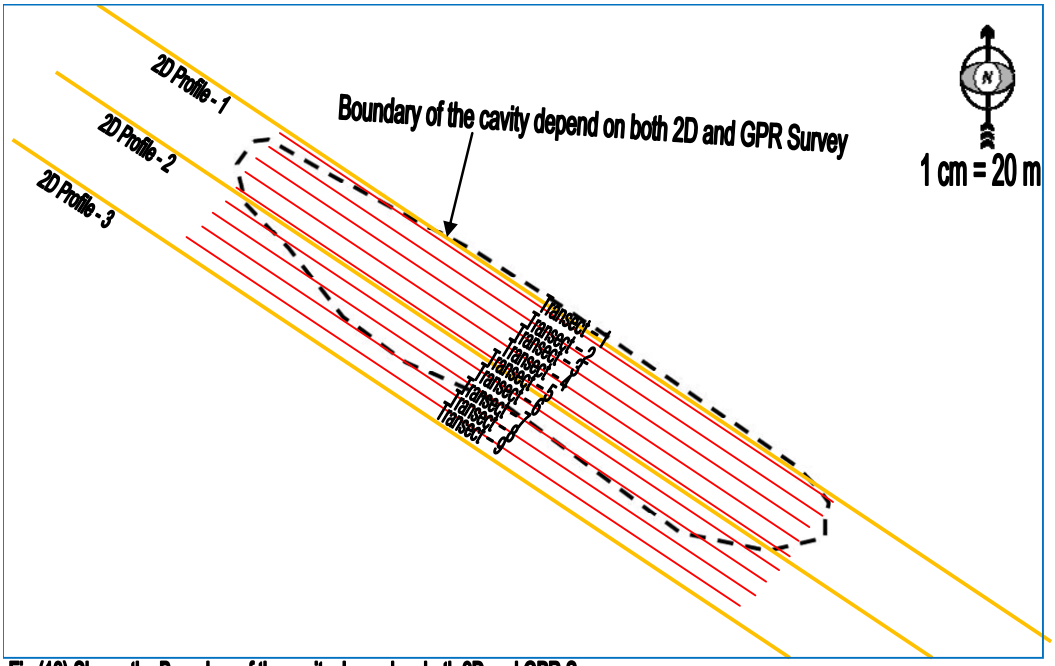

Fig (18) Shows the Boundary of the cavity depend on both 2D and GPR Survey